Robotica (2018) volume 36, pp. 1897–1919. © Cambridge University Press 2018
doi:10.1017/S0263574718000796

Unconventional calibration strategies for micromanipulation work-cells

G. Fontana†*, S. Ruggeri†, G. Legnani‡† and I. Fassi†

†*Institute of Intelligent Industrial Technologies and Systems for Advanced Manufacturing, National Research Council, 20133 Milan, Italy. Emails: serena.ruggeri@stiima.cnr.it, giovanni.legnani@unibs.it, irene.fassi@stiima.cnr.it*
‡*Department of Mechanical and Industrial Engineering, University of Brescia, 25123 Brescia, Italy*

(Accepted July 28, 2018. First published online: August 20, 2018)

SUMMARY
This paper presents and compares a set of calibration strategies useful to calibrate vision-based robotised work-cells for micromanipulation and microassembly. To grasp and release microparts precisely, robot calibration, camera calibration and robot-camera registration are needed. Conventional calibration methods are very onerous at the microscale, therefore, two alternative unconventional procedures, called virtual grid calibration and hybrid calibration, are developed for work-cells with high-performance robots, minimising necessary instrumentation. Moreover, an effective calibration of the robot end-effector is designed to compensate for misalignment and orientation errors with respect to the vertical rotational axis. This paper describes the calibration methods and their implementation, the results and the improvements achieved. A detailed comparison between the hybrid and the virtual grid calibrations is provided, demonstrating the higher performance of the latter strategy.

KEYWORDS: Micromanipulation, Calibration, Camera calibration, Work-cell accuracy, 2D vision systems.

1. Introduction

Automated work-cells have been recently designed and used to manipulate miniaturised components for different applications in growing fields, such as manufacturing and remanufacturing of electronic products, assembly of hybrid MEMS, microactuators, biomedical devices and ICT equipment.[1] These tasks require precise manipulation to grasp, orient and release parts. This manipulation is in the most cases performed on the x–y plane.

Although all devices composing a robotised work-cell present inaccuracies and introduce errors, they have to cooperate properly. This is especially relevant when manipulating and assembling components with sub-millimetric dimensions, in order to constitute small products. Therefore, the whole work-cell has to be calibrated. Stand-alone devices have to be calibrated and their relative location has to be univocally determined.[2]

This paper considers the errors related to vision systems (camera and lenses parameters and their location with respect to the robot) and the gripper, whereas manipulator errors are not considered. However, manipulator errors influence the implementation and later exploitation of the proposed calibration methods; therefore, the robot in the work-cell has to be characterised by good repeatability and by an accuracy, which is close to the application desired final precision. Repeatability depends on the mechanical quality of the robot; it is therefore a design and production property and cannot be improved. If the adopted robot is characterised by insufficient accuracy, it must be calibrated in advance with suitable procedures.[3–5] A short description of robot errors is briefly recalled in Appendix A. Differently, gripper errors have instead to be considered to comply with the end-effector later assembly.

* Corresponding author. E-mail: gianmauro.fontana@stiima.cnr.it

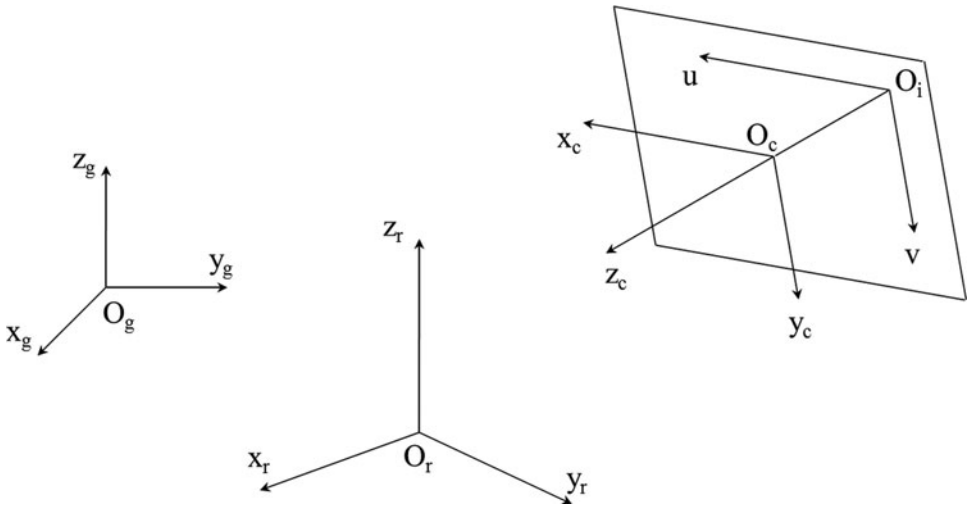

Fig. 1. Representation of the main reference frames involved in calibration processes.

Therefore, the main ideas of this work are as follows: (i) to develop and compare two different strategies for robot-camera calibration at microscale, which are called *hybrid* strategy (Section 5.1) and *virtual grid* strategy (Section 5.2), in order to show the superior potentialities of the virtual grid approach (Section 6.3); (ii) to apply the latest approach to both fixed (Section 6) and mobile cameras (Section 7); (iii) to develop effective end-effector calibration to finalize calibration of the whole work-cell (Section 8).

The non-conventional calibration strategies proposed are based on the well-known single-plane calibration model. However, novelty lies in the procedure and related implementation that target the microscale, which lacks standard and simple procedures. Moreover, single-plane calibration compensates for perspective and lens distortion errors resulting in a suitable approach in all cases, where precise manipulation is required in the *x*–*y* plane. These strategies can be implemented for calibration of all serial and parallel robots having from 2 to 4 degrees of freedom (dof) (two translations at least), mounting different types of grippers, such as vacuum grippers or microtweezers.

Therefore, the innovative aspect of this paper is the conception and comparison of calibration processes to co-register all individual devices at the same frame. The strategies thus developed have been then applied to the calibration of a micromanipulation work-cell, equipped with several cameras, assembly stages and a high precision micromanipulator mounting a vacuum microgripper.

This paper is structured as follows. After a brief discussion on the main issues related to robot and camera calibration in Section 2, Section 3 presents the conventional method to calibrate vision-based robotised work-cells. Section 4 describes a micro work-cell. In Section 5, the calibration procedures for fixed cameras proposed are presented, whereas Section 6 discusses on their implementation in our work-cell. Section 7 reports the calibration method and implementation for on-board cameras. Finally, end-effector calibration is reported in Section 8.

2. Robot and Camera Calibration Issues

When a robot and a vision system have to cooperate within the same working space, robot calibration, camera calibration and robot-camera registration are needed. Figure 1 shows the main reference systems involved during a general calibration process: the subscripts *g*, *r*, *c* and *i,* respectively, represent the ground, the robot base, the camera and the image. 3D space coordinates are indicated by *x*, *y*, *z* and expressed in millimetres, whereas *u* and *v* represent image coordinates and are expressed in pixels.

As said above, many applications require the manipulator to grasp and release objects on a planar surface under the supervision of a camera. In all these cases, 2D camera calibration, considering a single plane, is needed.

Camera calibration has to be performed to compute image pixel to real-world unit transformation and to compensate for perspective, distortion and spatial referencing errors[6,7] (Fig. 2).

https://doi.org/10.1017/S0263574718000796 Published online by Cambridge University Press

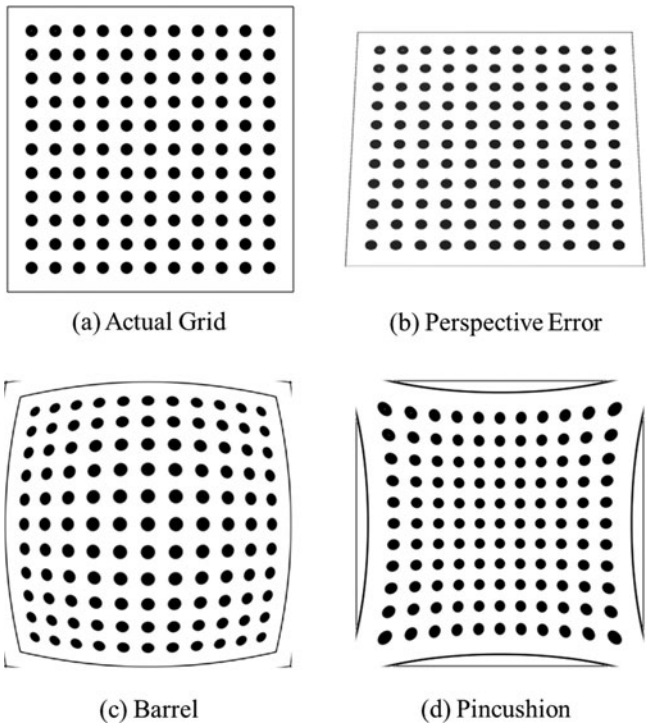

Fig. 2. Effect of different image distortions: (a) actual grid; (b) perspective error; (c) barrel; (d) pincushion. A perspective error can be compensated by the model of Eq. (B1), whereas radial and tangential distortion can be compensated by the model of Eq. (B2) in Appendix B.

3. The Conventional Calibration Strategy

In order to calibrate a camera, it is necessary to compare the real coordinates (generally expressed in millimetres) of some points with their coordinates in the camera image (in pixels). This operation exploits a model of the camera and lens, by applying perspective transformation, and distortion compensation. It can be performed by using an object of known shape and size. Planar 2D calibration can be performed by using a grid of points (also called *markers*). Good grids containing a set of precise shapes (usually circles) at predefined known positions are generally traced on flat rigid surfaces made of material which is not sensitive to external conditions, such as humidity, temperature or other. Common surfaces are special glass or ceramic plates.

Grid quality improves with the number and precision of the marked points and must fill most of the camera Field of View (FoV); moreover, it should be placed in focus.

The camera x–y reference system is generally established by placing its origin in the centre of one marker and the direction of one axis is chosen directing it to the centre of a second marker. The estimation of the relative pose of the camera with respect to the one of the robot (registration) is performed by moving a registration object mounted on the gripper (usually a pin) to some points of the grid. The absolute positions of the points in the robot reference system are then compared with the positions of the pin with respect to the grid in the camera reference system. Finally, the corresponding transformation is estimated; 3D cases require a third point to define the direction of a second axis. The last axis direction is achieved by imposing mutual orthogonality of the axes. As explained, 3D registration requires a minimum of 3 xyz points, whereas in 2D cases 2 xy points are sufficient. If more points are available, rototranslation can be identified with the least squares criteria. Camera and lens distortion models are reported in Appendix B.

At microscale, the mentioned procedure often used in the macro-domain is too onerous due to the characteristics of the vision system for the microscale and to more demanding precision. Indeed, to achieve a high level of resolution, in order to distinguish the maximum level of detail from images, the optics of the vision system must provide high magnification. This requirement causes the system to be characterised by a small FoV, thus limiting the viewable microassembly area. Moreover, high magnification requires a small working distance, which results in a small working volume for

https://doi.org/10.1017/S0263574718000796 Published online by Cambridge University Press

Table I. Technical data of the three vision systems.

	Camera model	Lens model (focal length f [mm])	Resolution (R) [pixel]	Field of view (FoV) [mm]	Spatial resolution (Rs) = FoV/R [μm/pixel]
Vision System 1 (bottom view)	Allied Prosilica GC2450	Voigtländer macro lens, f =100 mm	2448 × 2050	16.3 × 13.5	6.6
Vision System 2 (top view)	Allied Prosilica GC1380H	VS Technology VS-LD75, f =75 mm	1360 × 1024	32.70 × 24.59	24
Vision System 3 (on-board camera)	Matrix Vision mvBlueFOX-MLC205C	Matrix Vision MV-O-SMOUNT-12.0IRC B5M12028C, f =12mm	2592 × 1944	16.23 × 12.14	6.2

manipulation. Furthermore, under normal conditions of use (air, visible light, large numerical aperture and high magnification), the depth of field is fairly small, thus limiting the applicability of stereoscopic vision techniques (3D vision).[8] In addition, the calibration grid should be very precise (micrometric range), thus increasing its manufacturing cost. Furthermore, the registration pin must have highly precise construction and its location on the gripper must be established with high accuracy.

To overcome the abovementioned problems, two alternative unconventional calibration approaches (i.e., not conventional with respect to the calibration procedure used at macroscale) are proposed in this paper: virtual grid calibration and hybrid calibration. The conceived methods are implemented for the work-cell described in Section 4, but are adaptable to all the robotic work-cells designed for vision-based automatic manipulation on the x–y plane, irrespective of the kinematic structure of the manipulator, the gripper type and the overall setup.

It is important to stress that in many manipulation work-cells like the one analysed in this paper, a robot must operate with precision just in limited portions of its working space where it is necessary to register the x–y coordinate of the vision systems with the one of the manipulator. In our case each vision system has a FoV of few square centimetres (see Table I), whereas the robot working area is contained in a rectangle of roughly 15 cm × 10 cm. When a limited working area is considered for the robot and this is a precision manipulator, error distribution is similar to the one that can be produced by rototraslation, perspective transformation or optical distortion. These errors are easily compensated by camera calibration. Moreover, vision systems are generally used just to identify the pose of objects to be manipulated and not to perform any high precision dimensional analysis of objects. For these reasons, work-cell calibration can be performed without an external absolute reference system (e.g., a precision optical grid), but by using the robot itself as a reference. This is the principle adopted to design the virtual grid approach described in Section 5.2. After calibration, the final x–y coordinates of the robot and the vision systems will match (even if they could be possibly slightly different from the ones of an external absolute reference system, without obstructing the possibility of manipulating objects). This means that the implementation of the proposed virtual grid method is able to compensate for small errors correlated with robot accuracy (for significant errors robot calibration is needed). However, an exception occurs when the vision system is moved within a large area of the robot working space (i.e., on-board cameras mounted on a robot end-effector); in this case, the virtual grid method cannot compensate for the errors correlated with robot accuracy (even if they are small).

The hybrid calibration procedure proposed is described as a comparison in Section 5.1. The errors obtained in this case are worse, probably also because robot errors cannot be compensated.

4. The Work-Cell for Microassembly

The setup used for calibration experiments is reported in Fig. 3. The hardware and software concept of the work-cell is described in more detail in refs. [9, 10]. It consists of a high precision 4 dof robot Mitsubishi Electric[11] RP-1AH (1), with Schönflies motion[12] and vision systems meeting the

https://doi.org/10.1017/S0263574718000796 Published online by Cambridge University Press

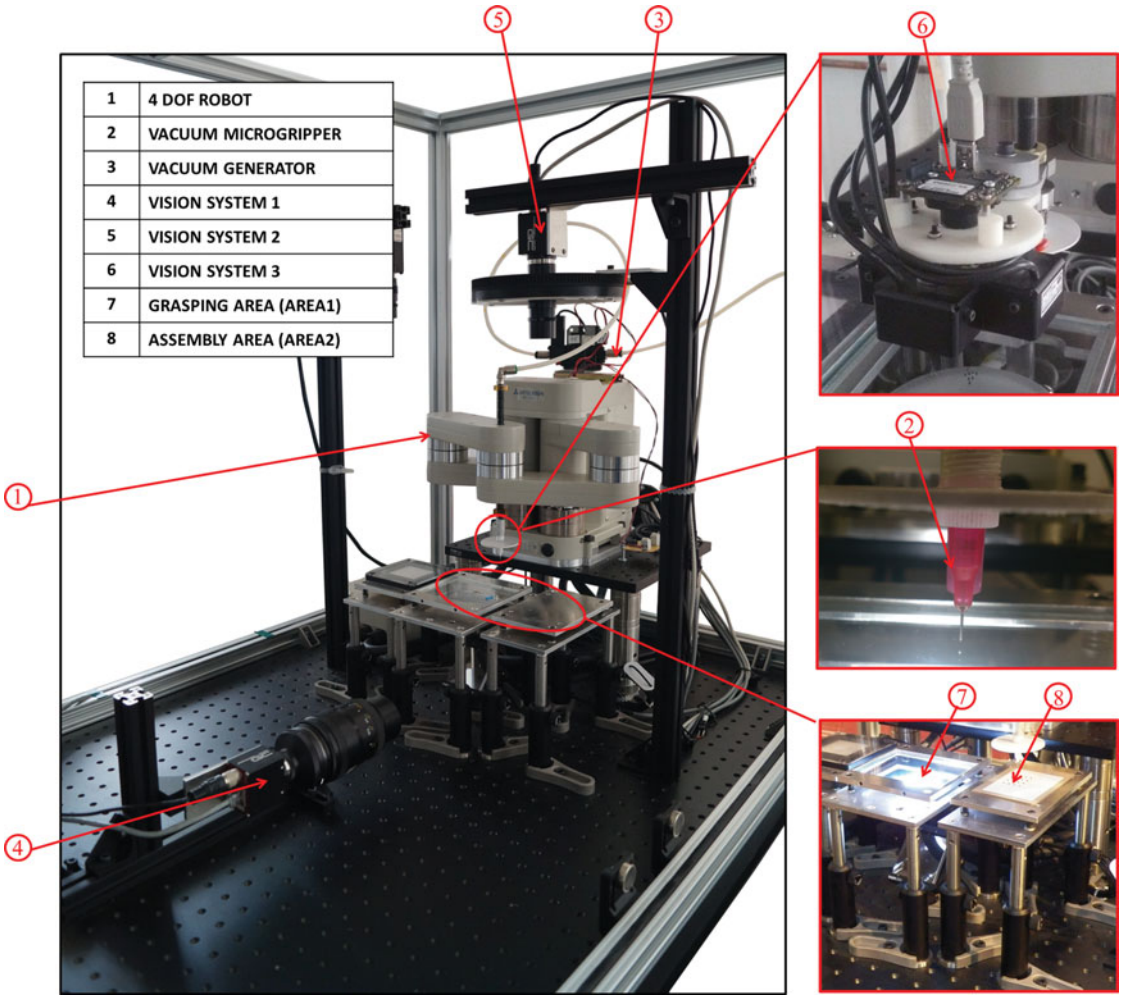

Fig. 3. The work-cell prototype.

microscale requirements of resolution, FoV, working distance, depth of field (see Table I) and gripping tools. In this case, a standard vacuum microgripper (2) with internal diameter size of 260 μm is used.

The robot x–y repeatability is ± 5 μm; its z repeatability is ± 10 μm. The vacuum generation system (3) exploits a vacuum ejector based on Venturi effect (3).

For the current purposes of this work, a work-cell is configured to exploit three suitable vision systems, including two fixed cameras (4, 5) and an on-board camera (6), in order to measure the pose of the parts in the focal plane. The technical data of these vision systems are reported in Table I. The parts to be manipulated lie on a transparent glass substrate (7), so that the first camera detects their position and orientation from the bottom by means of an optical mirror. The second camera allows instead a top view of the assembly area (8). The third camera is mounted on the robot end-effector, thus being able to move jointly with it and providing a top view of the whole working area.

As regards fixed cameras, calibration consists in determining the parameters to compensate for perspective transformation and optical distortion. As far as the mobile camera (on-board camera) is concerned, it is also necessary to determine its position with respect to the gripper. As to the gripper, misalignment and orientation errors with respect to the robot vertical rotational axis have to be identified.

The robot operates pick-and-place operations on a number of planar surfaces that have to be orthogonal to the robot vertical motion. Both the glass substrate and the assembly area (hereafter called area1 and area2) are mounted on compliant adjustable orientation platforms, in order to set their planarity and improve safety against any vertical accidental collision of the gripper on these areas. Planarity can be verified by using a precision laser sensor mounted on the robot end-effector.

https://doi.org/10.1017/S0263574718000796 Published online by Cambridge University Press

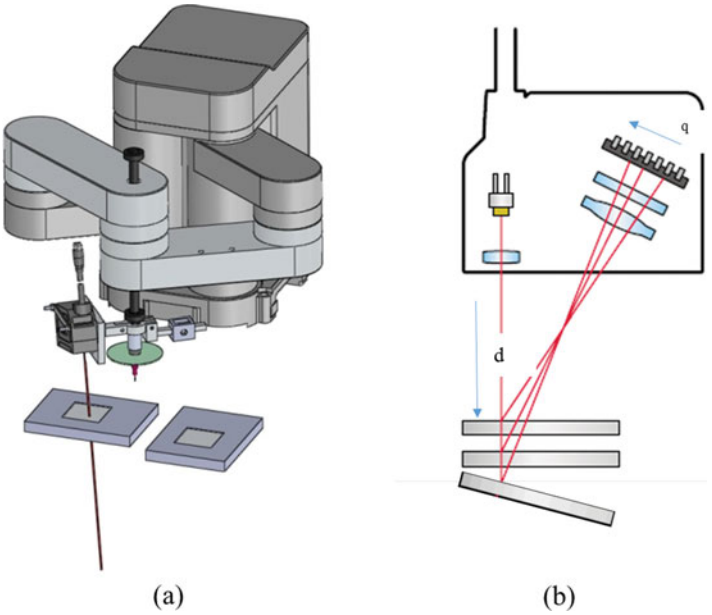

Fig. 4. Use of the laser sensor to verify planarity of the working areas and their orthogonality with respect to the robot vertical axis: (a) 3D model of the setup; (b) the working principle based on a linear array camera which measures the position of the incident beam reflected by the target $q = f(d)$.

Indeed, the orthogonality of the planes can be assured by adjusting the orientation of each plane by means of specific screws and it is verified by scanning the plane surfaces by a laser sensor (model IL-S065 by Keyence) moved by the robot (Fig. 4); a constant distance must be obtained.[13]

5. Non-Conventional Calibration Strategies for Fixed Cameras

A manipulator has to grasp and release objects in area1 and area2 under the supervision of vision systems (Fig. 3). In this specific case, the two areas are supervised by two fixed cameras, one for each zone, whereas an on-board camera will be considered later in Section 7. Thus, as said above, the robot has to be calibrated, as well as both the cameras; robot-camera registration is also needed. The aim of robot calibration is the improvement of its accuracy[14] and is performed by measuring its actual motion[3,15] to estimate its geometrical parameters.[4,5] In this work, it is assumed that the robot has shown suitable accuracy; therefore, this step is not discussed. However, calibration of the vision systems is necessary and 2D calibration is considered appropriate. Two different calibration strategies are proposed (main idea (i) in Section 1): the former represents an adjustment of the standard method, thus called hybrid strategy, whereas the latter is a fully non-traditional method and is named virtual grid strategy. It is worth noting that they are two alternative strategies to calibrate vision-based robotised work-cells for micromanipulation and microassembly; therefore, they are not combinable.

5.1. Hybrid calibration strategy

Camera calibration is performed by means of an actual grid of dots printed on a substrate and placed on a camera focal plane. The vision algorithms developed calculate in pixels the set of barycentres of the dots that, together with the corresponding set in millimetres, is processed by the camera calibration algorithm.

Afterwards registration between the robot base frame and the camera frame is needed.

Performing registration in the standard way is very challenging at microscale, due to a high-demanding positioning of the pin mounted on the end-effector on the grid points . Thus, depending on the configuration of the camera to be calibrated, two alternative approaches have been adopted.

Concerning area1, referencing is obtained by moving the gripper in the FoV of the camera in n known positions ($n \geq 2$). When a gripper nozzle cannot be easily recognised by the camera, a sphere gripped by the robot end-effector can be used. Similarly, in area2 registration of the second camera

https://doi.org/10.1017/S0263574718000796 Published online by Cambridge University Press

frame with respect to the robot frame is obtained by commanding the robot to place n spheres in the camera FoV in known positions. In both cases, the positions of the spheres are measured by the related camera by using its reference system and the corresponding transformation between the two systems is computed. Moreover, the rotation of the vertical axis has to be kept constant to avoid the influence of misalignment and orientation errors with respect to the vertical rotational axis of the robot (see Section 8).

5.2. Virtual grid calibration strategy

The virtual-grid calibration strategy is a methodology to simultaneously perform calibration of the camera and its registration with respect to the robot reference system without using any additional tools or sensors. The procedure is theoretically justified by the assumption that the robot positioning error is negligible, but in practice this procedure also compensates for small robot errors.

The physical grid is replaced by a "virtual grid" realized by objects placed by the robot in $N = R \times C$ known xy absolute positions (where R and C are the number of the rows and columns of the grid of points). In some cases, the gripper itself can suffice.

In practice, to calibrate the first camera (bottom view), the gripper is sequentially moved to the set of N positions, where a picture is taken and the position of the gripper (or of the object that the gripper holds) is measured by the vision system. In more detail, the procedure develops as follows. At the beginning the gripper is moved to the first x–y position (P_1), the camera takes a bottom picture of the gripper and the gripper position is measured. The pair of image coordinates and the gripper absolute coordinates is stored. The gripper is then moved in the x–y plane of a specified offset to reach position P_2. The camera takes a second picture and the gripper position is derived. These steps are repeated until the set of N grid positions is complete (see Figs. 5 and 6). The set of collected data is then elaborated by using the same principle of an ordinary grid, Eqs. (B1) and (B2) in Appendix B, thus compensating for distortion and perspective errors. A similar procedure is described in ref. [16]. To facilitate the measuring, the grasped object must have a simple shape and must be able to auto-centre on the gripper, to increase accuracy; for these reasons, a sphere can be considered suitable. When the gripper has a simple shape (e.g., a round nozzle), the bare gripper can be used for this calibration procedure. It is worth noting that the order of the collected data does not affect calibration precision, since the multidirectional positioning error is inferior to robot repeatability (5 μm in the x–y plane).

As regards the second camera (top view), the procedure must be adapted because of the presence of the robot itself in the camera FoV. In this case, the robot is employed to grasp several objects and place them in the camera FoV, in predefined $N = R \times C$ positions, to form a grid (see Fig. 7). In our case, small spheres are placed on an adhesive surface to avoid undesired part rolling. Figure 5 shows the flowcharts of the described virtual grid calibration strategies for area1 and area2.

In both cases, the gripper is kept with constant orientation (no rotation around the vertical axis) to avoid any effects due to the geometrical inaccuracy of the gripper itself, that will be considered in Section 8.

This procedure does not require any use of expensive calibrated grid, or any other calibration tools, and final precision depends only on the vision system spatial resolution and the encoder resolution of the robot.

5.3. Performance evaluation

The verification test to measure the effectiveness of the different calibration procedures is performed by asking the robot to place some objects (e.g., the gripper nozzle or some spheres) in known xy positions within the camera FoV, by measuring their positions by means of a comparison if the known positions with the measured ones. The objects are placed in verification positions different from the ones used for calibration.

For the sake of completeness, this calculation has been computed also for the points used for registration in the hybrid process and for the virtual grid construction in the second process. The chosen performance index is the radial position error e, defined as

$$e = \sqrt{(x_a - x_d)^2 + (y_a - y_d)^2}$$

https://doi.org/10.1017/S0263574718000796 Published online by Cambridge University Press

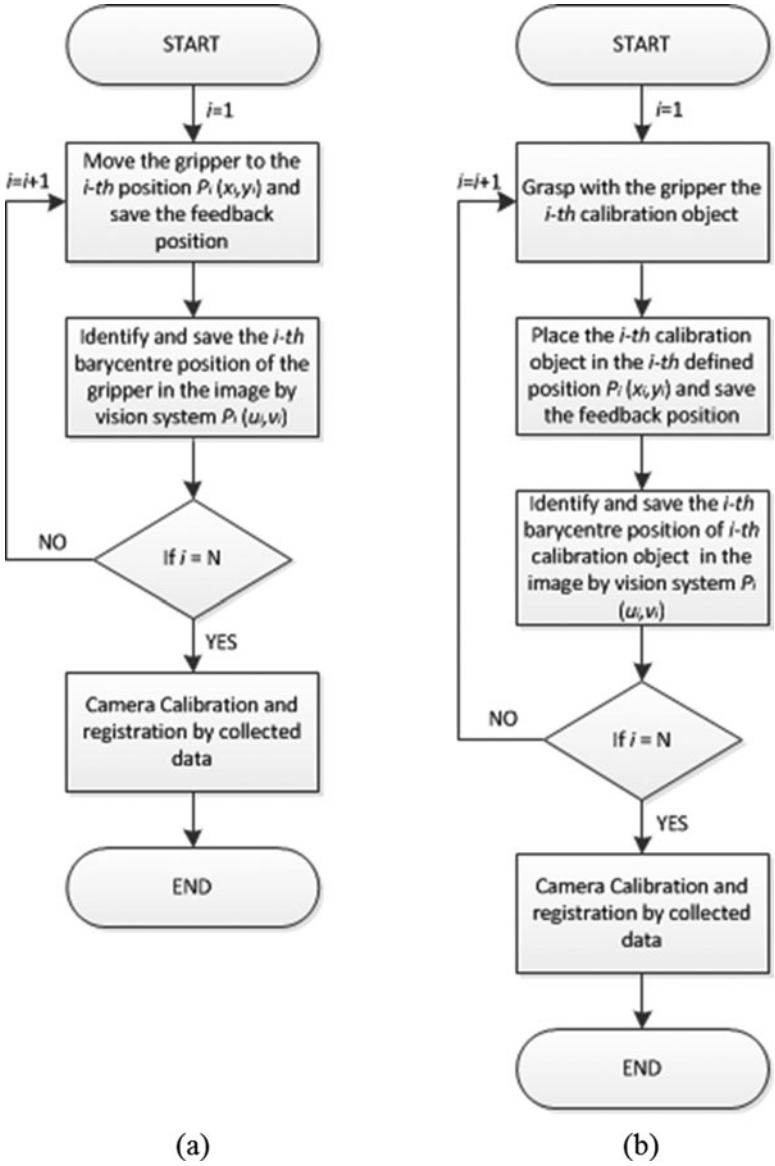

Fig. 5. Flowcharts illustrating the steps of virtual grid calibration implementation: (a) for area1; (b) for area2.

where x_a, y_a are the actual coordinates of the gripper nozzle or sphere centre and x_d, y_d are the coordinates measured by the calibrated camera. Figure 8 shows the radial position error (e) in the calibration points of area2 represented by arrows: errors have been amplified for a clear visualisation.

6. Implemented Calibration Strategies

6.1. Calibration of area1

In this Section, the implementation of the two different approaches to the calibration of the first camera and its registration with respect to the robot base frame are presented.

6.1.1. Hybrid strategy. As prefaced in Section 3, camera calibration is performed by means of an actual grid. In this case, a grid of 8×7 black dots printed on a white substrate with a diameter of 1 mm, a dot spacing of 2 mm and a dot spacing tolerance of 5 μm is adopted. The grid is fixed on the glass substrate and placed to be seen in focus. The camera takes a picture of the grid and the vision algorithm provides for the identification of the dots and the calculation of their barycentres.

https://doi.org/10.1017/S0263574718000796 Published online by Cambridge University Press

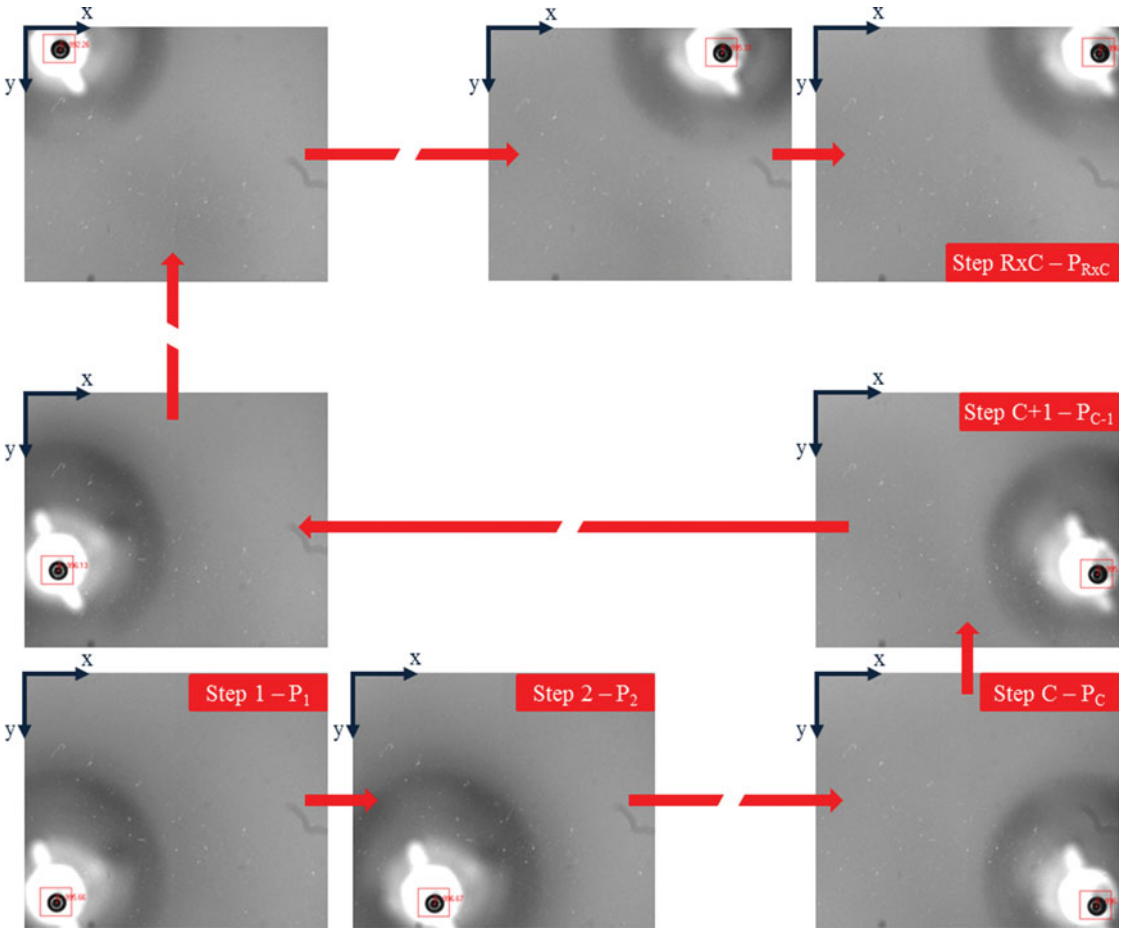

Fig. 6. Schematic representation of the different steps of virtual grid calibration in area1.

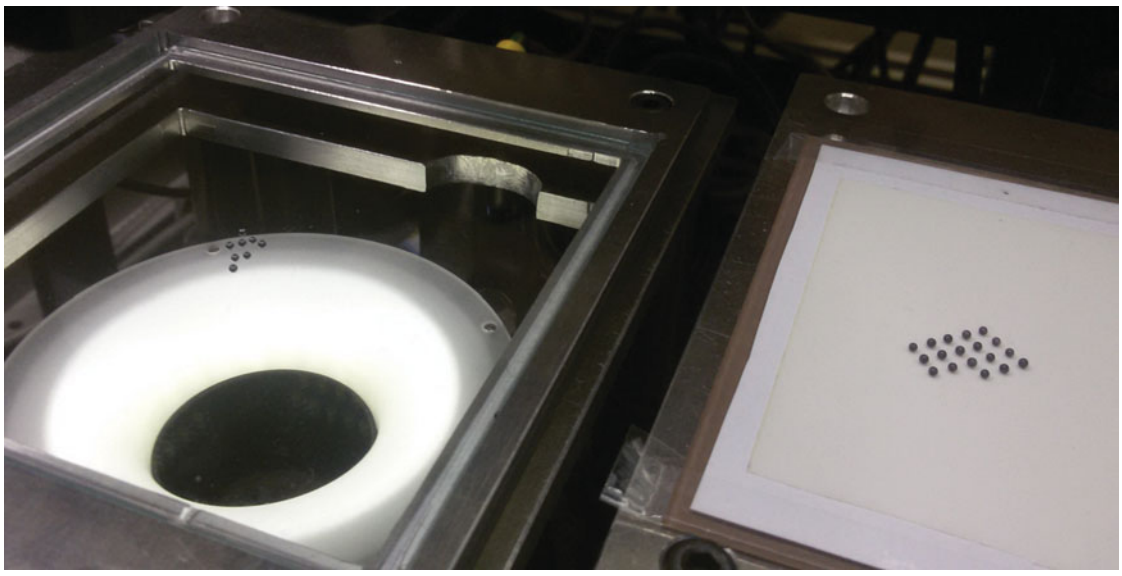

Fig. 7. Calibration of the second camera. On the left, area1 used as a gripping area seen by the first camera; on the right, virtual grid under construction in area2.

https://doi.org/10.1017/S0263574718000796 Published online by Cambridge University Press

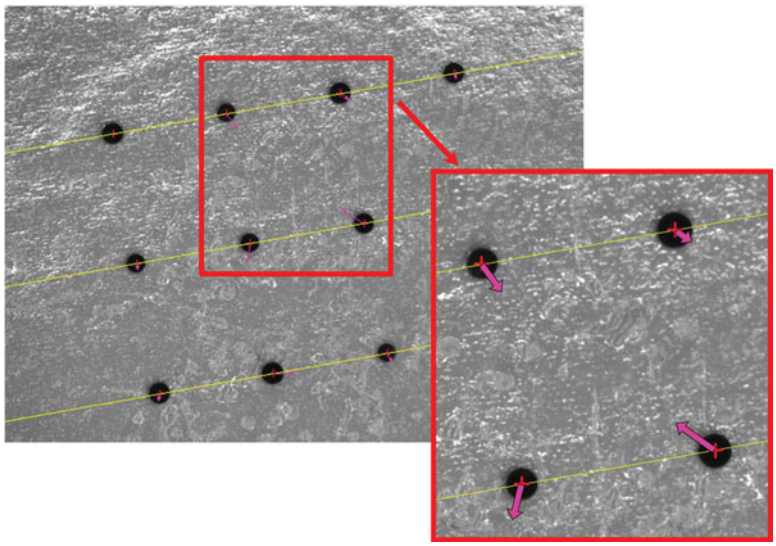

Fig. 8. Representation of the radial position error e in the calibration points of area2.

The origin of the calibration grid coordinate system is set to coincide with the barycentre of the top left dot; the x-axis is aligned with the topmost row of dots and the y-axis isorthogonal and directed downwards in the image. In this way, the two sets of barycentre positions expressed in millimetres and pixels can be processed by a calibration algorithm. Afterwards, the algorithm performs the transformation and compensates for perspective and distortion errors. For this work, all the vision algorithms are developed using LabView^{TM}; its vision libraries are based on the concept of Eqs. (B1) and (B2)[17] and provide a calibration function where different types of error compensation can be selected. In this case, aiming at the highest vision system performance, a kind of calibration taking into account both perspective and distortion errors is chosen.

To perform registration, the robot grasps a glass sphere of about 1 mm diameter (with a diameter tolerance of ± 0.2 mm) and moves it to $n = 4$ ($n \geq 2$) known positions in the x–y plane. For all these positions, the z height is kept constant so that the sphere can be seen in focus: in this way, the offset between the registration and calibration planes falls into the camera depth of field, which has an order of magnitude of 1 mm for the first camera. At each position, the robot stops, the feedback position is sent from the robot controller to the master personal computer and the camera takes an image. The developed vision algorithm provides for the identification of the sphere in the FoV. Then, the algorithm performs the calculation of its barycentre in pixels and, since the camera is already calibrated, also in millimetres. Therefore, the corresponding transformation between the camera and the robot reference systems can be computed by estimating the parameters (ϑ, x_0, y_0) of the planar rototranslation matrix between the two reference systems, represented by the following relation:

$$\begin{bmatrix} x_r \\ y_r \end{bmatrix} = \begin{bmatrix} \cos(\vartheta) & -\sin(\vartheta) \\ \sin(\vartheta) & \cos(\vartheta) \end{bmatrix} \begin{bmatrix} x_c \\ y_c \end{bmatrix} + \begin{bmatrix} x_0 \\ y_0 \end{bmatrix} \tag{1}$$

At first, an initial estimation ϑ_e of the angle ϑ is obtained by considering the coordinates of two points of the grid measured in the camera and in the robot space:

$$\vartheta_e = \text{atan2}\,(y_{r2} - y_{r1},\ x_{r2} - x_{r1}) - \text{atan2}(y_{c2} - y_{c1},\ x_{c2} - x_{c1})$$

where atan2(y, x) is the 4-quadrant extension of arctan(y/x). Then, a first estimation of x_0, y_0 is obtained by the coordinate of one point in the grid and the robot space as:

$$\begin{bmatrix} x_0 \\ y_0 \end{bmatrix} = \begin{bmatrix} x_r \\ y_r \end{bmatrix} - \begin{bmatrix} \cos(\vartheta_e) & -\sin(\vartheta_e) \\ \sin(\vartheta_e) & \cos(\vartheta_e) \end{bmatrix} \begin{bmatrix} x_c \\ y_c \end{bmatrix}$$

https://doi.org/10.1017/S0263574718000796 Published online by Cambridge University Press

The estimation is then improved by an iterative procedure which considers all the points of the grid. Linearising Equation (1) in the neighbourhood of $\vartheta = \vartheta_e$ (where ϑ_e is the first estimation of the angle ϑ), one obtains

$$\begin{bmatrix} x_r \\ y_r \end{bmatrix} = \begin{bmatrix} (-\sin(\vartheta_e)x_c - \cos(\vartheta_e)y_c) & 1 & 0 \\ (\cos(\vartheta_e)x_c - \sin(\vartheta_e)y_c) & 0 & 1 \end{bmatrix} \begin{bmatrix} \Delta\vartheta \\ x_0 \\ y_0 \end{bmatrix} + \begin{bmatrix} \cos(\vartheta_e)x_c - \sin(\vartheta_e)y_c \\ \sin(\vartheta_e)x_c + \cos(\vartheta_e)y_c \end{bmatrix}$$

that for the *ith* point of the grid can be synthetically written as

$$B_i = \begin{bmatrix} x_{ri} \\ y_{ri} \end{bmatrix} - \begin{bmatrix} \cos(\vartheta_e)\, x_{ci} - \sin(\vartheta_e)\, y_{ci} \\ \sin(\vartheta_e)\, x_{ci} + \cos(\vartheta_e)\, y_{ci} \end{bmatrix}$$

$$A_i = \begin{bmatrix} (-\sin(\vartheta_e)\, x_c - \cos(\vartheta_e)\, y_c) & 1 & 0 \\ (\cos(\vartheta_e)\, x_c - \sin(\vartheta_e)\, y_c) & 0 & 1 \end{bmatrix}$$

$$L = \begin{bmatrix} \Delta\vartheta \\ x_0 \\ y_0 \end{bmatrix}.$$

All the n collected data are then grouped in the matrices A and B:

$$B = \begin{bmatrix} B_1 \\ \vdots \\ B_i \\ \vdots \\ B_n \end{bmatrix} \qquad A = \begin{bmatrix} A_1 \\ \vdots \\ A_i \\ \vdots \\ A_n \end{bmatrix}.$$

Therefore, by applying the Least Square Method to the collected data, it is possible to derive the estimated values of the vector parameters $L = [\Delta\vartheta, x_0, y_0]^{\mathrm{T}}$ from equation

$$L = (A^T A)^{-1} A^T B = A^+ B$$

where A^+ is the Moore–Penrose pseudo-inverse matrix of the coefficient matrix A ($2n$ x 3) and B is the ($2n$ x 1) vector of the known terms. Therefore, we obtain $\vartheta = \vartheta_e + \Delta\vartheta$. Since linearisation introduces errors, the estimation of $\Delta\vartheta, x_0, y_0$ can be reiterated to improve calibration.

Moreover, to avoid the effects of geometric errors at the end-effector, the rotation of the vertical axis is kept constant to an angle $\alpha = \alpha_{\mathrm{cal}}$ during this phase. Geometric errors at the end-effector will be considered in Section 8.

The results obtained with this approach are reported in Table II, which shows the absolute values of the mean and maximum errors and the RMS error.

6.1.2. Virtual grid strategy. As described above, the procedure is based on the use of a virtual grid. The robot is firstly commanded to position the gripper nozzle or the sphere to be seen in focus by the camera. After that, the cycle of movements and images captures starts, until the grid is complete. Again, a grid of 8×7 positions is used and end-effector orientation is kept constant.

As for hybrid strategy, the positions of the barycentres of the gripper nozzle or the sphere are identified and, again, the origin of the coordinate system of the calibration grid is set to coincide with the barycentre of the top left dot. However, in this case, this point corresponds to a specific position achieved by the robot, thus registration between the robot and camera reference frames is simultaneously provided.

The statistical information of mean, maximum and RMS errors calculated for a single complete grid is reported in Table II. Both the results for the points used for calibration and verification points are reported.

https://doi.org/10.1017/S0263574718000796 Published online by Cambridge University Press

Table II. Results of calibration strategies applied to area1 and area2.

		Error in calibration points [μm]				Error in non-calibration points [μm]			
		Mean error	Max error	RMS error	No. of points	Mean error	Max error	RMS error	No. of points
Area 1	Hybrid C.	15.2	43.2	10.5	56(+4*)	14.2	50.4	11.9	56
	Virtual Grid C.	3.9	8.8	1.7	56	6.3	19.0	3.1	
Area 2	Hybrid C.	67.5	128.3	36.0	192(+4*)	62.7	103.1	31.5	12
	Virtual Grid C.	6.8	20.8	4.8	12	19.5	46.2	12.3	

*The number in parentheses represents the points used for registration in case of hybrid calibration (n for area1 and m for area2).

6.2. Calibration of area2

Hereby, the hybrid and "virtual grid" strategies are addressed for calibration and referencing of the camera providing a top view of the assembly area.

6.2.1. Hybrid strategy. The same physical standard grid used for the first camera is adopted. The camera takes a picture of the 16×12 black dots grid which is processed by the vision algorithm.

The registration of the camera frame with respect to the robot frame is then obtained by commanding the robot to place $m = 4$ ($m \geq 2$) spheres in the camera FoV in unaligned positions.

To accomplish this task, the first already calibrated camera is exploited to provide the robot with the x–y coordinates in its reference system of the spheres lying in area1.

The robot then picks and places the spheres in the specified positions of the second camera FoV. The spheres barycentres are then calculated in the camera reference frame and transformation with respect to the robot frame can be computed.

The procedure for the evaluation of the calibration error for the second camera is identical to the previous one. Calibration quality is checked by placing some spheres in some points different from the ones used for registration and the measuring error is evaluated. Table II reports the results obtained.

6.2.2. Virtual grid strategy. In practice, the process to create the grid of spheres is similar to the approach used for the first camera registration. A grid of 4×3 dots is considered as suitable, since it provides an amount of data which is more than a sufficient and a relatively low execution time, which is an important aspect if re-calibration of the system is frequently needed. The robot picks and places, one by one, the spheres in the FoV of the camera to be calibrated. For each sphere deposition the camera takes a picture of the under-construction grid. Once the last placed sphere has been detected, its pixel barycentre is calculated. The data are then used to calibrate the second camera by applying the same mathematical approach used for the first camera. The position errors obtained with this strategy are reported in Table II.

6.3. Comparison between hybrid and virtual grid calibration strategies

Concerning the unconventional calibration methods applied to the different areas, the results obtained are reported in Table II. As one can notice, the virtual grid strategy is more effective than the hybrid one, in terms of both mean, maximum and RMS errors. The mean error in the verification positions with the virtual grid approach applied to area1 is less than half of the one obtained with the hybrid approach. The same error for area2 is even 3 times lower.

An analysis of the two calibration strategies leads to an evaluation of the different sources of errors. Concerning hybrid calibration, the total error is given by a combination of errors deriving both from camera calibration and from its registration. In particular, camera calibration is affected by the dot spacing tolerance of the grid and by the error committed by the vision algorithm detecting the dot barycentres. In registration a considerable error arises because of an offset between registration and the calibration planes, which cannot be neglected without the use of high-precision devices. This makes the mean and maximum errors in the registration points to be comparable with the ones in non-registration points, oppositely to what happens in the virtual grid strategy case. Moreover, the use of the robot to move the gripper nozzle or the spheres involves a further error due to the encoder

https://doi.org/10.1017/S0263574718000796 Published online by Cambridge University Press

resolution affecting the robot feedback position reading besides robot geometric errors. Again, an error associated to the barycentre identification (of the gripper nozzle or the sphere) by the vision algorithm occurs. In the specific case of the first camera, a small error in the auto-centring of the sphere gripped by the robot end-effector can affect the process. When the gripper nozzle is easily recognised by the camera and the sphere is not necessary, this error does not arise. In the second camera case, the auto-centring error adds to the error in positioning the sphere on the adhesive substrate caused by a subtle collision between the gripper and the substrate itself.

On the other side, since in the virtual grid calibration strategy camera calibration and its registration are performed simultaneously, fewer sources of error than in the previous strategy arise. In this case, errors due to encoder resolution and vision algorithm performance occur. The error associated to the sphere auto-centring can occur when the first camera is calibrated, and, as regards the second camera, an additional error in positioning the spheres arises.

To support the calibration of area2, it is established that the already calibrated camera 1 be exploited: on the other hand, a mechanically fixed reference place where spheres are picked up can also be adopted. This choice is done to neglect the use of external devices.

It is worth noting that the gripper nozzle diameter and the sphere diameter are not influential parameters and do not need to be precisely known in advance. Only in the case of area2 calibration, it is essential to check the sphere diameter in order to avoid mechanical interference among the placed spheres.

By applying the virtual grid method to fixed cameras, high precision can be achieved despite small errors of the manipulator (influencing accuracy), since this method provides a "mapping" between the robot and the camera reference systems. On the other side, even if the hybrid method is affected by small robot errors, its precision can be improved by preliminary robot calibration, if needed.

To conclude this discussion about different calibration strategies, besides a performance analysis in terms of precision, investigation on the feasibility of calibration execution is fundamental. Comparing the two strategies in terms of execution time, the virtual grid approach is slower than the other one, since grid construction takes time: with reference to the area1 calibration, if the execution of the hybrid strategy takes some seconds (8 sec in the case of 4 registration points), the construction of a 8×7 virtual grid takes about 2 min. This difference is due to the definitely fewer positions needed for registration than for the virtual grid calibration strategy, since the necessary time for taking an image of the physical grid of dots is negligible. Furthermore, the necessary time to calibrate area2 is always much higher than the one needed to calibrate area1, regardless of the method adopted, since both virtual grid construction and registration derive from a pick and place operation. For example, in the case of a 4×3 virtual grid construction in area2, execution time is about 3 min (note that, compared to the virtual grid of area1, 50% more time is necessary to build a grid of one-fifth of positions). As to hybrid strategy, the registration of area2 by using four positions takes about 1 min, that is, eight times more than with the first one. In all cases, note that time can vary depending on how fast the vision system recognises the spheres.

The economic aspect is also relevant: an accurate actual grid can be expensive; the hybrid approach thus requires higher costs than the virtual grid strategy. Indeed, the price of a commercial grid can be two orders of magnitude higher than the one of some glass spheres.

7. On-Board Camera Calibration

As described in Section 4, the work-cell is equipped with a mobile camera mounted on the robot end-effector. In order to exploit this additional vision system, camera calibration and robot-camera registration are required. If the camera pose is known with respect to the gripper, when the camera measures the relative positions of some points (in millimetres), it is possible to determine the absolute position of those points. Ideally, the camera rotates around a vertical axis centred in the nominal gripper position. Whereas we may assume by the construction of a precision manipulator and by the working planes planarity (see Section 4) that the axis is vertical, we cannot assure that this axis crosses exactly the gripper nominal centre. The D location of the vertical axis is thus to be determined. This is a simplified case of the more general case of solving the well-known $AX{=}XB$ problem.[18]

For this camera, only the virtual strategy is implemented since it leads to better results, if compared with the hybrid one (main idea (ii) in Section 1). The procedure to collect the data is very similar to the

https://doi.org/10.1017/S0263574718000796 Published online by Cambridge University Press

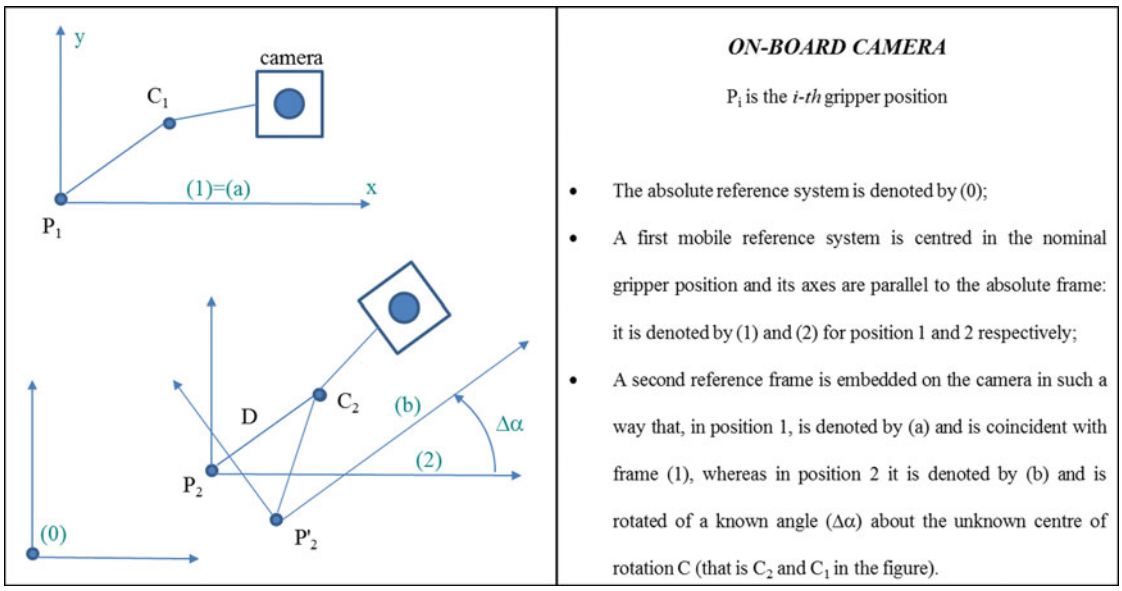

Fig. 9. Definition of the reference frames for on-board camera calibration.

one adopted by the second vision system for area2. Indeed, even in this case, the robot is commanded to place a grid of n spheres on the robot working area.

The robot is then moved to a position P_1 $(x_{g1}, y_{g1}, \alpha_1)$. A picture of the grid is taken and, for each point, the corresponding coordinates in the robot space (x_i, y_i) and in the camera space (u_{1i}, v_{1i}) are collected.

The robot is then moved to a second position P_2 $(x_{g2}, y_{g2}, \alpha_2)$ with a second rotation angle $(\alpha_1 \neq \alpha_2)$; a second picture is taken and a new measure of the camera coordinates of the points (u_{2i}, v_{2i}) is collected. It is worth noting that $\Delta\alpha = \alpha_2 - \alpha_1$ should have a value to make the effect of the rotation clearly visible e.g., $\Delta\alpha > 10^\circ$.

The relative frames are defined in Fig. 9.

The relative position of ith point with respect to the gripper in position 1 is

$$A_{(1)i} = \begin{bmatrix} x_{r1i} \\ y_{r1i} \end{bmatrix} = \begin{bmatrix} x_i - x_{g1} \\ y_i - y_{g1} \end{bmatrix}$$

Camera parameters can be obtained by the data $A_{(1)i}$ and (u_{1i}, v_{1i}) collected in pose 1.

Using these parameters and the camera coordinates (u_{2i}, v_{2i}) of the points in pose 2, a new relative position $A_{(2)i}$ of the points with respect to the camera is obtained.

Considering the first gripper pose, the absolute position of the grid point is

$$A_{(0)i} = P_1 + A_{(a)i}$$

And, considering the second gripper pose, it is also

$$A_{(0)i} = P_2' + RA_{(b)i} \tag{2}$$

$$P_2' = C_2 + R\,(P_2 - C_2) \tag{3}$$

where the rotation matrix R is

$$R = \begin{bmatrix} \cos(\Delta\alpha) & -\sin(\Delta\alpha) \\ \sin(\Delta\alpha) & \cos(\Delta\alpha) \end{bmatrix}$$

https://doi.org/10.1017/S0263574718000796 Published online by Cambridge University Press

Table III. Estimated centres of rotation.

D	c*	c2	c3	c4	c5	c6
x [μm]	−0.6	90.1	25.9	−26.2	53.2	−12.4
y [μm]	213.7	286.7	207.7	198.3	222.8	248.2

and the D location of the vertical axis is

$$D = C_1 - P_1 = C_2 - P_2.$$

Therefore, by representing the 2×2 identity matrix with I, one obtains

$$(R - I)\,D = P_2 - P_1 + RA_{(b)} - A_{(a)} \tag{4}$$

and the unknown D can be finally found by

$$D = (R - I)^{-1}(P_2 - P_1 + RA_{(b)} - A_{(a)})$$

with

$$R' = R - I = \begin{bmatrix} \cos(\Delta\alpha) - 1 & -\sin(\Delta\alpha) \\ \sin(\Delta\alpha) & \cos(\Delta\alpha) - 1 \end{bmatrix} \quad (R - I)^{-1} = \frac{1}{2}\begin{bmatrix} -1 & -\frac{\sin(\Delta\alpha)}{\cos(\Delta\alpha)-1} \\ \frac{\sin(\Delta\alpha)}{\cos(\Delta\alpha)-1} & -1 \end{bmatrix}.$$

If more than two poses are considered, and/or more points are considered for each pose, Eq. (4) can be written for any combination of point and pose, and the equations can be grouped obtaining an over-constrained linear system to be solved with the least square criteria

$$\bar{R}\,D = \bar{H} \quad \text{with} \quad \bar{R} = \begin{bmatrix} R_1 - I \\ \vdots \\ R_k - I \\ \vdots \end{bmatrix} \quad \bar{H} = \begin{bmatrix} \vdots \\ P_k - P_1 + R_k A_{(b)k} - A_{(a)k} \\ \vdots \end{bmatrix}$$

$$D = \left(\bar{R}^{\,T}\bar{R}\right)^{-1}\bar{R}^{\,T}\,\bar{H} = \bar{R}^{\,+}\,\bar{H}$$

where $\bar{R}^{\,+}$ is the Moore–Penrose pseudo-inverse of $\bar{R}$.

After calibration, the absolute position of any point j measured for any gripper pose k may be performed by combining Eqs. (2) and (3):

$$A_{(0)j} = P_k + (I - R_k)\,D + R_k A_{(b)j} \tag{5}$$

The centre of the rotations is estimated six times (Table III). In five cases ($c2$–$c6$), the estimation is based on one of the poses $p2$–$p6$ with respect to the first pose $p1$, used for camera calibration and registration, so that case c_l refers to the pose p_l, with l =2, ..., 6. In the last case (c*), all the poses are considered and the centre is estimated with the least square criteria considering all the five poses ($p2$–$p6$).

Tables IV, V and VI report the results of a calibration test based on 6 poses and 20 points for each pose (Fig. 10). The performance is tested by applying an error index based on Eq. (5):

$$E_{jk} = P_k + (I - R_k)\,D + R_k A_{(b)j} - A_{(0)j}$$

As shown in the tables, the centre of the rotation determined by considering just one pose (cases $c2$–$c6$) allows for better results on that individual pose (see the combination c_l, p_l on the diagonal highlighted in the tables). However, the rotation centre determined with the least square criteria on all the poses (case c*), on average, performs better. Its error is close to the minimum and generally

https://doi.org/10.1017/S0263574718000796 Published online by Cambridge University Press

Table IV. RMS error in the cross-reference test for the calculation of the rotation centre.

E_{rms} [μm]	c*	c2	c3	c4	c5	c6	Min	Max
p2	26.2	16.6	24.3	30.4	21.0	25.3	16.6	30.4
p3	22.5	41.1	20.4	27.6	23.2	28.3	20.4	41.1
p4	28.1	79.2	36.1	23.4	49.0	35.6	23.4	79.2
p5	18.8	20.7	17.1	21.7	16.2	20.3	16.2	21.7
p6	20.1	33.6	22.9	22.2	25.5	17.7	17.7	33.6

Table V. Maximum error in the cross-reference test for the calculation of the rotation centre.

E_{max} [μm]	c*	c2	c3	c4	c5	c6	Min	Max
p2	46.1	35.0	42.2	51.2	36.8	46.5	35.0	51.2
p3	45.4	77.3	42.9	51.6	53.8	55.3	42.9	77.3
p4	61.7	121.9	72.2	46.3	88.3	69.0	46.3	121.9
p5	45.6	42.0	41.0	50.2	42.2	47.9	41.0	50.2
p6	51.9	65.5	58.4	49.8	62.3	44.1	44.1	65.5

Table VI. Mean error in the cross-reference test for the calculation of the rotation centre.

E_{mean} [μm]	c*	c2	c3	c4	c5	c6	Min	Max
p2	23.9	14.3	22.1	28.2	18.9	23.1	14.3	28.2
p3	20.1	38.2	17.8	25.3	20.5	25.4	17.8	38.2
p4	24.9	77.1	33.1	20.7	46.3	31.3	20.7	77.1
p5	15.3	18.5	13.0	18.8	12.1	17.6	12.1	18.8
p6	16.9	31.6	20.1	19.2	22.9	14.3	14.3	31.6

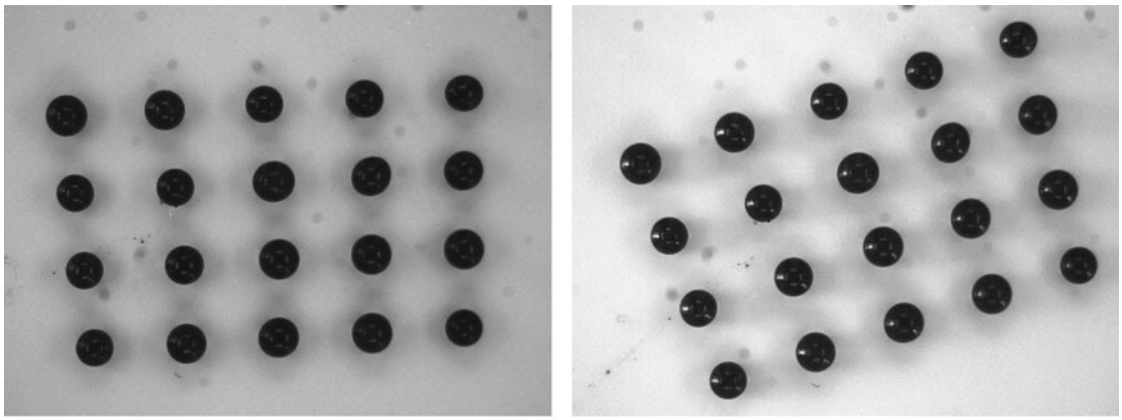

Fig. 10. Images of the grid taken from two different gripper positions: (a) pose 1; (b) pose 6.

far from the maximum. Figure 11 shows the radial position error in the calibration points seen by the on-board camera in *p*6 calculated with the rotation centre determined with the least square method.

In the virtual grid calibration strategy, camera calibration and its registration are performed simultaneously, as in the previous cases. Different sources of error have to be considered. Since this procedure is similar to the one of the second vision system looking at area2, all the errors arising in that case apply to this case. Moreover, since the camera moves with the robot, the robot pose accuracy influences the results. Indeed, camera calibration is performed in a limited robot working area but is then exploited in the whole area, where the robot performance can change. For this reason, differently from the case of fixed cameras, the virtual grid method applied to the on-board camera

https://doi.org/10.1017/S0263574718000796 Published online by Cambridge University Press

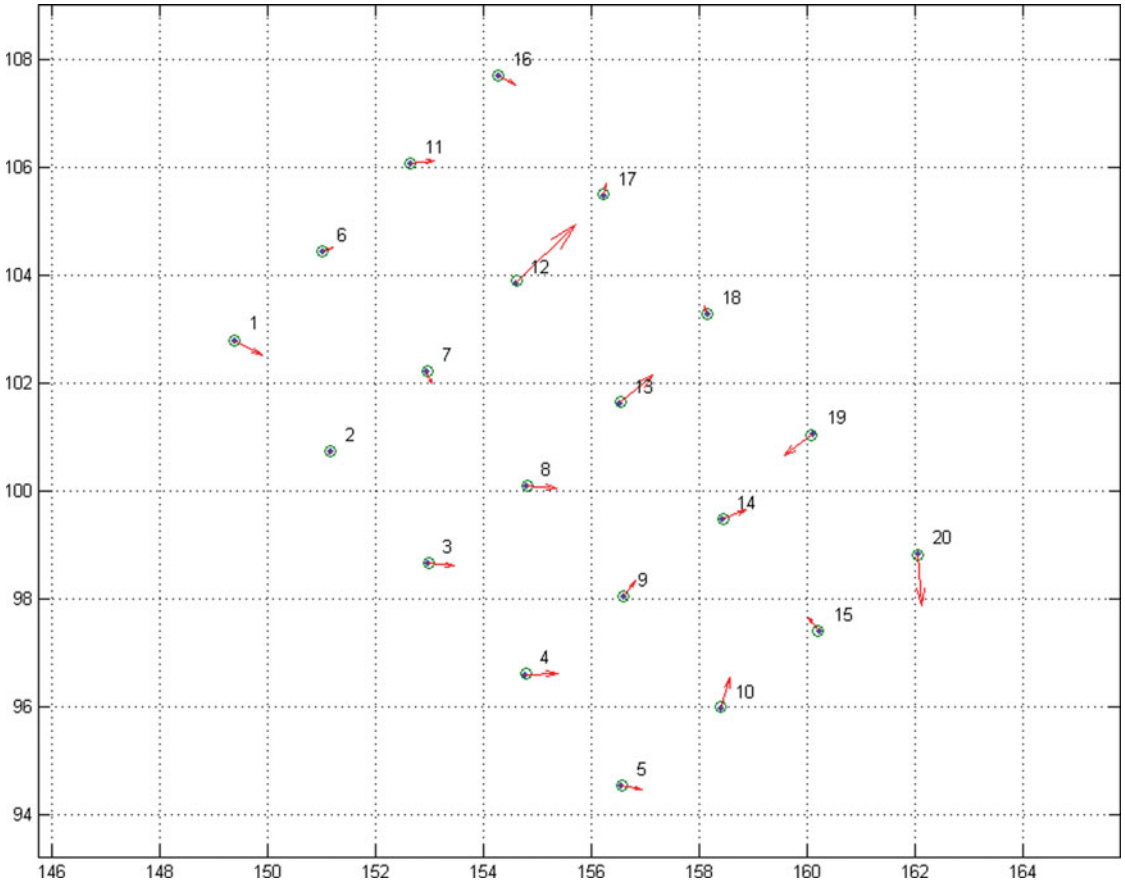

Fig. 11. Representation of radial position error in the calibration points seen by an on-board camera in *p6*.

cannot compensate for even small errors correlated with robot accuracy. Therefore, to guarantee the method precision preliminary robot calibration is needed.

8. End-Effector Calibration

When the robot is commanded to pick or release a part with a different orientation with respect to the one adopted to calibrate the camera, a position error can be observed.

It was verified that the error is due to a geometric error of the gripper (Fig. 12). Therefore, an easy and effective kinematic calibration of the robot end-effector is devised to enhance accuracy (main idea (iii) in Section 1). This calibration exploits the setup available in area1 able to provide a microgripper bottom view. Indeed, the already calibrated and georeferenced camera 1 is considered as a suitable measurement system for the robot end-effector position.

It is worth noting that gripper calibration can be performed after the calibration of the vision systems, because in these cases manipulation operations are performed with a fixed orientation of the gripper. The gripper errors are simply compensated by an extra x–y translation with an amplitude depending on the gripper orientation.

In the following, the error model is reported together with experimental implementation and results.

8.1. The error model

Misalignment and orientation errors with respect to the manipulator vertical rotational axis can affect the microgripper, thus causing inaccurate manipulation of microcomponents. Figure 12 compares the ideal and the actual cases. In the former case, when commanding an α rotation about the vertical axis of the robot, a simple rotation of the microgripper is obtained: therefore, there is no displacement in the x–y plane. In latter case, since the gripper centre does not belong to the rotation axis, gripper rotation induces a displacement in the x–y plane.

https://doi.org/10.1017/S0263574718000796 Published online by Cambridge University Press

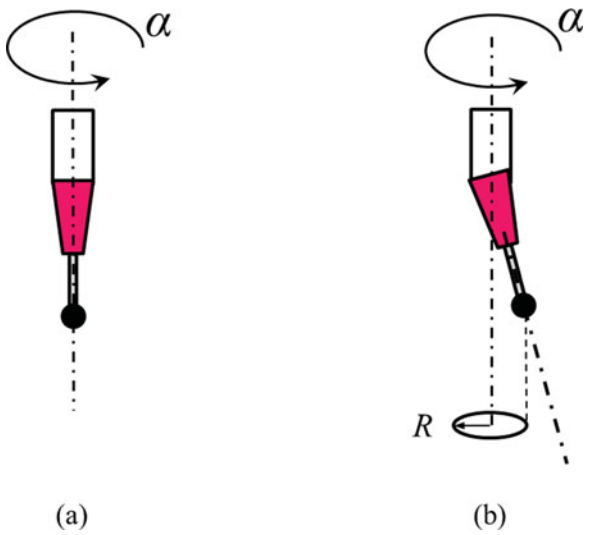

Fig. 12. The end-effector error: (a) ideal model; (b) error affected model.

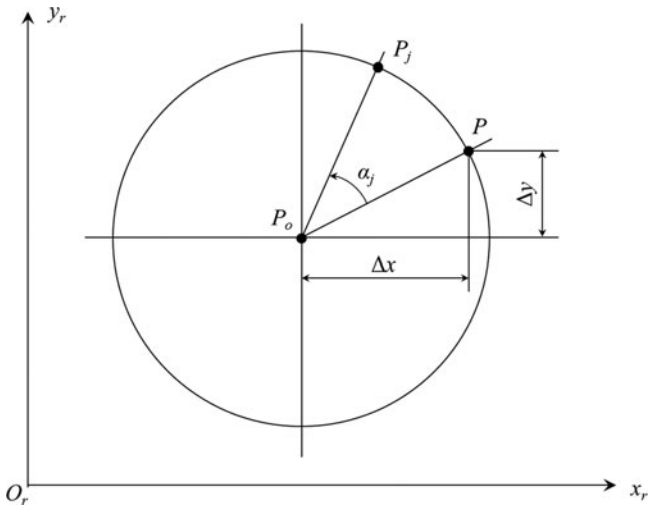

Fig. 13. Reference model for end-effector calibration.

Following an analysis of the system, the use of a rigid model to describe gripper deformation is considered as suitable. If a set of angular displacements is commanded by keeping the end-effector x, y and z positions constant of, the gripper nozzle barycentres (or the picked sphere barycentres) detected by the vision system 1 should lay on a circumference whose centre belongs to the vertical axis. Therefore, it is possible to derive a reference model as the one shown in Fig. 13, where the bottom view of the robot end-effector by vision system 1 is considered.

Indicating with α_{cal} the end-effector rotation angle used during the camera calibration process and with $P = [x, y]^{\text{T}}$ the corresponding planar position of the end-effector, lying on the circumference of radius R and centre $P_o = [x_o, y_o]^{\text{T}}$ belonging to the rotation vertical axis:

$$\begin{bmatrix} x \\ y \end{bmatrix} = \begin{bmatrix} x_o \\ y_o \end{bmatrix} + \begin{bmatrix} \Delta x \\ \Delta y \end{bmatrix}$$

where Δx and Δy represent the microgripper misalignment with respect to P_o when $\alpha = \alpha_{\text{cal}}$.

https://doi.org/10.1017/S0263574718000796 Published online by Cambridge University Press

If we rotate the end-effector of the angle α_j relative to α_{cal}, this will achieve the new position $P_j = [x_j, y_j]^{\text{T}}$:

$$\begin{bmatrix} x_j \\ y_j \end{bmatrix} = \begin{bmatrix} x_o \\ y_o \end{bmatrix} + \begin{bmatrix} \cos(\alpha_j) & -\sin(\alpha_j) \\ \sin(\alpha_j) & \cos(\alpha_j) \end{bmatrix} \begin{bmatrix} \Delta x \\ \Delta y \end{bmatrix}$$

Thus, the position error ΔP_j due to the misalignment results as

$$P_j - P = \begin{bmatrix} \Delta x_j \\ \Delta y_j \end{bmatrix} = \begin{bmatrix} \cos(\alpha_j) - 1 & -\sin(\alpha_j) \\ \sin(\alpha_j) & \cos(\alpha_j) - 1 \end{bmatrix} \begin{bmatrix} \Delta x \\ \Delta y \end{bmatrix}$$

Or, shortly, as

$$\Delta P_j = A_i \begin{bmatrix} \Delta x \\ \Delta y \end{bmatrix}$$

In such model Δx and Δy are unknown constant parameters to be estimated for compensating for the described error with no hardware changes and enhancing the system accuracy. The parameters actual values can be determined by applying the Least Square Method to a set of different achieved positions on the circumference. It is possible to group the measure of the gripper position error for n points as

$$\Delta P = \begin{bmatrix} \Delta P_1 \\ \vdots \\ \Delta P_i \\ \vdots \\ \Delta P_n \end{bmatrix} \qquad A = \begin{bmatrix} A_1 \\ \vdots \\ A_i \\ \vdots \\ A_n \end{bmatrix}$$

and to solve the system with the least square criteria as

$$\begin{bmatrix} \Delta x \\ \Delta y \end{bmatrix} = A^{+} \Delta P$$

It is worth noting that by increasing the number of the rotations and the considered points, a better estimation could be obtained.

8.2. Experimental implementation and results

The robot end-effector is rotated over 360° with a step of 20°: this means that 18 rotations about the vertical axis are performed. The previously executed camera calibration cannot completely eliminate the errors in the image acquired by the camera, therefore, it is decided that the series of rotations are repeated in a number of different positions in the camera FoV, trying to improve the calibration process performance. For this reason, a grid of 30 positions (6×5) is chosen. The process steps are as follows:

1. The end-effector holding a sphere is commanded to the first grid position with the angle used for camera 1 calibration.
2. Camera 1 takes a picture of the sphere, calculates and records its position.
3. The end-effector rotated of the specified step angle (20°).
4. Steps (2) and (3) are repeated to span 360°.
5. The end-effector is moved to the second (or the following) grid position with the calibration angle.
6. Steps (2)–(5) are repeated until the last rotation in the last grid position.

An over-constrained system of equations is obtained by rewriting the equation of ΔP_j for all the considered gripper poses. The system is linear in the unknowns Δx and Δy; as a result they can be easily estimated by the Least Mean Square method (see Table VII). This makes the compensation of their effect possible by means of a geometric model.

https://doi.org/10.1017/S0263574718000796 Published online by Cambridge University Press

Table VII. Estimated values of end-effector calibration parameters.

Δx [μm]	Δy [μm]	$R = \sqrt{\Delta x^2 + \Delta y^2}$ [μm]
−68.7	137.2	153.44

Table VIII. Results of end-effector calibration (in all, two grids of 30 positions each and 18 rotations per position are considered).

Error before calibration [μm]			Error after calibration [μm]		
Mean error	Max error	RMS error	Mean error	Max error	RMS error
188.8	309.3	109.7	11.8	30.0	6.2

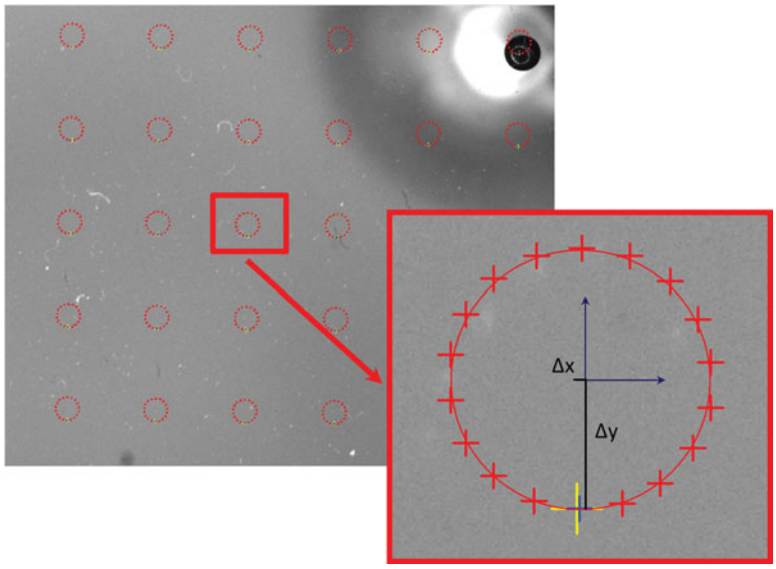

Fig. 14. The experimental points considered in the end-effector calibration.

In order to assess the calibration process effectiveness, the final mean, maximum and RMS position error values are measured before and after the correction in 30 positions different from the ones chosen for the calibration process and scattered in the working area (Fig. 14). Table VIII shows the results obtained: in particular, the first three columns in the table report the errors that would be obtained if a position is achieved with different orientations ignoring the correction. As one can see, the errors without the use of the end-effector calibration are an order of magnitude higher than the ones with the end-effector calibration. Thus, a significant enhancement of the performance is achieved.

An important aspect is represented by the need of a calibrated vision system to support the actual implementation of end-effector calibration. Thus, both from a conceptual and an operational point of view, end-effector calibration is addressed subsequent to the calibration of area1. For this reason, the main error source is area1 calibration error, which adds to the errors due to the encoder resolution, robot geometric errors, vision algorithm performance and auto-centring of the sphere (when a sphere is used).

The execution time of end-effector calibration can take several minutes: for example, a 6×5 grid with 18 rotations for each position can be executed in 12–13 minutes. Obviously, as the number of points in the calibration grid or the step in the series of the end-effector rotations increase, time will increase proportionally. However, the number of points can be reduced.

https://doi.org/10.1017/S0263574718000796 Published online by Cambridge University Press

9. Conclusions

This paper presents different calibration strategies applied to a micromanipulation work-cell. Two methods for camera calibration and camera-robot registration are compared and critically analysed. The virtual grid approach demonstrates higher efficiency as compared to the hybrid calibration strategy, both from a performance and an economic point of view. Indeed, the mean error in verification positions with the virtual grid approach is less than half compared to the one obtained with the hybrid approach, and the equipment price (i.e., some glass spheres) is two orders of magnitude lower than the one of a commercial grid. Moreover, the developed kinematic end-effector calibration procedure allows for a significant improvement of the overall system accuracy: the error decreases more than an order of magnitude. The techniques proposed are general and can be applied to general micromanipulation work-cells that use robots up to 4 dof and fixed or mobile 2D vision systems. In particular, the implementation of these calibration techniques has been preparatory for the execution of different micromanipulation and microassembly tasks, such as the mounting of mechanical microcomponents, the placement of electronic components on printing circuit boards, and the testing of microgrippers to evaluate their performance.

Calibration procedures do not require any additional equipment, as they exploit only micromanipulation work-cell devices: a robot, a gripper and vision systems, together with auto-centring objects (e.g., microspheres) to be manipulated. On the contrary, the laser sensor used to assure the orthogonality of the planes and the optical calibration grid necessary to perform the hybrid calibration are optional devices. This benefits the work-cell overall cost since they are task-specific and can be rather expensive.

Acknowledgements

This work has been partially funded by the Italian Ministry for University and Research (MIUR) and by Regione Lombardia under the framework of the 3AQ Regione Lombardia-CNR.

References

1. J. Cecil, M. B. Bharathi Raj Kumar, Y. Lu and V. Basallali, "A review of micro-devices assembly techniques and technology," *Int. J. Adv. Manuf. Technol.* **83**(9), 1569–1581 (2016).
2. K. Schröer, "Precision and Calibration," **In:** *Handbook of Industrial Robotics*, 2nd ed. (S. Y. Nof ed.) (Wiley & Sons Inc., New York, 1999) pp. 795–810.
3. G. Legnani, C. Mina and J. Trevelyan, "Static calibration of industrial manipulators: Design of an optical instrumentation and application to SCARA robots," *J. Robot. Syst.* **13**(7), 445–460 (1996).
4. A. Omodei, G. Legnani and R. Adamini, "Calibration of a measuring robot: Experimental results on a 5 DOF structure," *J. Robot. Syst.* **18**(5), 237–250 (2001).
5. B. W. Mooring, Z. S. Roth and M. R. Driels, *Fundamentals of Manipulator Calibration* (John Wiley & Sons, Inc, New York, 1991).
6. Z. Zhang, "A flexible new technique for camera calibration," *IEEE Trans. Pattern Anal. Mach. Intell.* **22**(11), 1330–1334 (2000).
7. J. G. Fryer and D. C. Brown, "Lens distortion for close-range photogrammetry," *Photogramm. Eng. Remote Sens.* **52**, 51–58 (1986).
8. S. Ruggeri, G. Fontana and I. Fassi, "Chapter 9: Micro-assembly," **In:** *Micro-Manufacturing Technologies and Their Applications: A Theoretical and Practical Guide* (I. Fassi and D. Shipley eds.) (Springer International Publishing, 2017) pp. 223–259.
9. G. Fontana, "Assembly at the Microscale: Design and Implementation of a Robotised Work-Cell," *Ph.D. Thesis* (University of Brescia, 2014).
10. S. Ruggeri, *Advanced Robotic Applications: Performance Improvement Techniques for Industrial Robots Acting at the Macro- and Micro-Scale* (Scholar's Press, Germany, 2013) pp. 177–240.
11. Mitsubishi website: http://www.mitsubishi-automation.co.uk/.
12. O. Bottema and B. Roth, *Theoretical Kinematics* (Dover Publications Inc., New York, 1979) pp. 312–315.
13. G. Legnani, A. Gabrielli, A. Ousdad, I. Fassi, S. Ruggeri and G. Fontana, "A Laser Calibration Device for Mini Robots," *Proceedings of the ASME 2015 International Design Engineering Technical Conferences & Computers and Information in Engineering Conference IDETC/CIE 2015*, Boston, Massachusetts, USA (2015).
14. ISO 9283:1998, "Manipulating industrial robots - Performance criteria and related test methods," 2nd Edition (www.iso.org, International Organization for Standardization, Geneva, Switzerland, 1998) pp. 1–60. Technical Committee: ISO/TC 299 Robotics. ICS: 25.040.30 Industrial robots. Manipulators.
15. ISO/TR 13309:1995, "Manipulating industrial robots - Informative guide on test equipment and metrology methods of operation for robot performance evaluation in accordance with ISO 9283," (1995), 1st Edition

(www.iso.org, International Organization for Standardization, Geneva, Switzerland, 1995), pp. 1–15. Technical Committee: ISO/TC 299 Robotics. ICS: 25.040.30 Industrial robots. Manipulators.
16. B. Tamadazte, S. Dembélé and N. Le Fort-Piat, "A multiscale calibration of a photon videomicroscope for visual servo control: Application to MEMS micromanipulation and microassembly," *Sensors & Transducers J.* **5**(Special Issue), 37–52 (2009).
17. G. Bradski and A. Kaehler, "Chapter 11: Camera Models and Calibration," **In:** Learning OpenCV (M. Loukides ed.) (O'Reilly Media, Inc., Sebastopol CA, USA, 2008) pp. 370–404.
18. I. Fassi and G. Legnani, "Hand to sensor calibration: A geometrical interpretation of the matrix equation AX=XB," *J. Robot. Syst.* **22**(9), 497–506 (2005).
19. I. Fassi, G. Legnani, D. Tosi and A. Omodei, "Chapter 8: Calibration of Serial Manipulators: Theory and Applications," **In:** *Industrial Robotics: Programming, Simulation and Applications* (L. K. Huat ed.) (Intech, Book, 2006).
20. G. Legnani, D. Tosi, R. Adamini and I. Fassi, "Chapter 9: Calibration of Parallel Kinematic Machines: Theory and Applications," **In:** *Industrial Robotics: Programming, Simulation and Applications* (L. K. Huat ed.) (Intech, Book, 2006).
21. L. G. Shapiro and G. C. Stockman, *Computer Vision* (Prentice-Hall, Englewood Cliffs, NJ, 2002).

Appendix A: Manipulator Errors

Errors in the manipulator structure determine an error in the gripper pose that can be represented mainly by two performance indexes: accuracy and repeatability.[14] Accuracy depends on constant sources of errors like geometric inaccuracy and encoders offset, whereas repeatability is affected by random errors (mainly mechanical backlash). Accuracy errors can be predicted and compensated by suitable calibration techniques,[3–5] in order to get closer to the application desired final precision. In general, the end-effector pose (position and orientation) S can be expressed in function of the joint coordinate vector Q and of the structural parameters L as:

$$S = f(Q, L) \cong f(Q_n, L_n) + \frac{\partial f}{\partial Q}\Delta Q + \frac{\partial f}{\partial L}\Delta L$$

where f is the direct kinematics function, the subscript n marks the nominal values and Δ marks the deviation from the nominal situation. On the basis of suitable models[19,20] and of experimental data, it is possible to estimate the error ΔL of the unknown parameters and compensate for them with a suitable variation of the joint coordinates ΔQ. Calibration can be performed by the final user or directly at the factory by the manufacturer for an extra cost.

Appendix B: Camera and Lens Distortion Models

Perspective errors occur when the camera axis is not orthogonal to the object under inspection. To limit the perspective error, the camera should be positioned as orthogonally as possible to the planar surface, however, this error has to be compensated to compute the image pixel to real-world unit transformation. Moreover, distortion errors are introduced by lens imperfections. Typically, a camera lens introduces radial distortion, that is, the image information is misplaced relatively to the optical centre of the lens.[7]

Since cameras can be described by the pin-hole model,[21] the 2D perspective correction is based on the following equations:

$$\begin{cases} x = \dfrac{au' + bv' + c}{gu' + hv' + 1} \\ y = \dfrac{du' + ev' + f}{gu' + hv' + 1} \end{cases} \tag{B1}$$

where, after the distortion correction, x and y represent the position in the real-world of one feature in the image whose coordinates in pixels are u' and v', and a, b, c, d, e, f, g, h are suitable constants to be determined by calibration.

https://doi.org/10.1017/S0263574718000796 Published online by Cambridge University Press

The optical distortion[17] can be modelled by suitable polynomials in the distance r of the considered image point from the centre of distortion u_c, v_c:

$$\begin{bmatrix} u' \\ v' \end{bmatrix} = \begin{bmatrix} u \\ v \end{bmatrix} + \left(1 + k_2 r^2 + k_4 r^4 + \cdots\right) \begin{bmatrix} u'' \\ v'' \end{bmatrix} + \begin{bmatrix} 2a'v'' + b'\left(r^2 + 2u''^2\right) \\ 2a'\left(r^2 + 2v''^2\right) + 2b'u'' \end{bmatrix}$$
$$r^2 = u''^2 + v''^2 \quad \begin{bmatrix} u'' \\ v'' \end{bmatrix} = \begin{bmatrix} u - u_c \\ v - v_c \end{bmatrix} \tag{B2}$$

where k_{2i} ($i \in \mathrm{N}^*$) and *a'* and *b'* are constants to be experimentally determined.

https://doi.org/10.1017/S0263574718000796 Published online by Cambridge University Press